Radiative decay of topologically disordered excitons

Ningjun Wang,[a] Annabel A. Muenter,[b] and Shaul Mukamel[c]
Center for Photoinduced Charge Transfer, Department of Chemistry, University of Rochester, Rochester, New York 14627

(Received 13 May 1993; accepted 26 May 1993)

We calculate the time resolved fluorescence from a topologically disordered two-dimensional molecular aggregate smaller than an optical wavelength. The photon emission rate is expressed in terms of a configurationally averaged particle-hole Green's function, calculated using the ladder diagram approximation. The exciton coherence size at a given energy is shown to be equal to the average oscillator strength per state, provided the superradiance decay rate is much smaller than the absorption linewidth. The variation of the coherence size with molecular density and with exciton energy across the band is explored.

I. INTRODUCTION

The radiative dynamics of molecular aggregates and superlattices is an area of intensive current interest.[1–9] The time resolved fluorescence of molecular aggregates may show effects of cooperative spontaneous emission. We denote the fluorescence radiative decay rate of the aggregate by $N_{\text{eff}}\gamma$, γ being the radiative decay rate of a single molecule and N_{eff} is the coherence size. The concept of a coherence size was first advanced by Mobius and Kuhn[3] in analyzing the dependence of fluorescence quenching on the acceptor surface density for a system consisting of an acceptor monolayer on top of a *J*-aggregate monolayer. For an ordered aggregate in which the molecules occupy a regular lattice (without disorder or dephasing) and whose size is much smaller than the optical wavelength, N_{eff} increases linearly with N (the number of molecules in the aggregate).[1,2] For infinite size aggregates (larger than the optical wavelength of excitation λ), N_{eff} is equal to $(\lambda/a)^d$, a being the lattice constant and d is the dimensionality for $d=1$ (Refs. 10,11) and $d=2$.[12,13] Grad *et al.*[10] have calculated the coherence size for the radiative decay rate using the Haken–Strobl model[14] for homogeneous dephasing. It was shown that the cooperativity is quenched by dephasing and that the coherence size varies from $(\lambda/a)^d$ for an infinite aggregate with no dephasing, to unity for large dephasing. Spano and Mukamel[2] have calculated the effect of static inhomogeneous broadening on the radiative lifetime of rigid aggregates using a reduced equation of motion for the density matrix. They showed how the coherence size decreases with inhomogeneous broadening. The effect of exciton–phonon coupling on the coherence size was studied as well; as the aggregate size is increased, the coherence size was shown to approach a limiting value, determined by the exciton–phonon coupling strength.[1] These studies suggest that disorder and dephasing destroy the cooperativity among molecules and reduce the coherence size.

Recent experiments involving mixed monolayers of cyanine dyes (*J*-aggregates)[8,9] have pointed out the need for a quantitative understanding of the role of topological disorder on the radiative coherence size. In this paper we calculate the time resolved fluorescence of this system for the case where no relaxation occurs between the various exciton states in the *J*-aggregate band. The radiative decay will be treated using an effective Hamiltonian (the superradiance master equations).[10,15,16] We then use Green's function techniques to incorporate the disorder.[17] The present approach generalizes the previous treatments in which the calculated coherence size was averaged over all single exciton energies and did not carry any information regarding its dependence on exciton energy. Here on the other hand, we calculate explicitly its dependence on exciton energy. The aggregate size is assumed to be much smaller than the optical wavelength of excitation but larger than the maximum coherence size. We show that the coherence size at a given exciton energy is equal to the average oscillator strength per state at that energy[18] only when the super-radiance decay rate is much smaller than the inhomogeneous broadening. We calculate the energy dependent coherence size, explore its variation with the density of molecules, and show how the maximum coherence size is diminished by topological disorder. For *J*-aggregates, in which the nearest-neighbor interaction is negative, the maximum coherence size N_c is found to be at the band edge. We further find that N_c increases with density.

II. GREEN'S FUNCTION EXPRESSION FOR FLUORESCENCE FROM A MOLECULAR ASSEMBLY

Consider a lattice where a fraction $c\equiv N/M$ of the lattice sites are occupied by molecules, N being the number of molecules and M the number of sites. The molecules are assumed to have two electronic levels with a ground state $|g\rangle$ and an excited state $|e\rangle$ separated by the energy gap $\hbar\Omega$. The two states have no permanent electric dipole, and

[a]University of Rochester, Department of Physics, Rochester, New York 14627.
[b]Photographic Research Laboratories, Eastman Kodak Company, Rochester, New York 14652.
[c]University of Rochester, Department of Chemistry, Rochester, New York 14627.

 0021-9606/93/99(5)/3604/10/$6.00

the transition between them is electric dipole allowed. The molecules are coupled by dipole–dipole interactions and their transition dipole moments μ are aligned in the same direction. In one experimental realization of such a system,[8] the occupied sites contain dye molecules with an energy gap in the visible spectral region, while the "unoccupied" sites are filled with similarly shaped spacer molecules having a significantly larger energy gap.

Our calculation of the fluorescence line shape starts with the following Hamiltonian:

$$H=H_{\rm eff}+H_{\rm int}, \tag{1}$$

$H_{\rm eff}$ is the effective Hamiltonian of the exciton system which includes radiative decay and can be derived using projection operator techniques.[19–21] For a given configuration of molecules it reads[1,10]

$$H_{\rm eff}=H_{\rm ex}-i\hat{\Gamma}, \tag{2}$$

where

$$H_{\rm ex}=\sum_{\mathbf{r}}\epsilon_{\mathbf{r}}B_{\mathbf{r}}^{+}B_{\mathbf{r}}+\sum_{\mathbf{r},\mathbf{r}'}{}'J(\mathbf{r}-\mathbf{r}')B_{\mathbf{r}}^{+}B_{\mathbf{r}'}, \tag{3}$$

is the material Hamiltonian of the exciton system, $\Sigma'_{\mathbf{r},\mathbf{r}'}$ denotes summation of $\mathbf{r}$ and $\mathbf{r}'$ over all lattice sites excluding $\mathbf{r}=\mathbf{r}'$. $B_{\mathbf{r}}^{+}$ and $B_{\mathbf{r}}$ are the creation and annihilation operators of exciton at site $\mathbf{r}$

$$B_{\mathbf{r}}^{+}|0\rangle=|\mathbf{r}\rangle, \tag{4}$$

where $|0\rangle$ denotes the ground state (i.e., all sites are in their ground state), and $|\mathbf{r}\rangle$ denotes the state in which only site $\mathbf{r}$ is excited and all other sites are in their ground state. $H_{\rm ex}$ conserves the number of excitons, which is the consequence of the Heitler–London approximation.[22] $\epsilon_{\mathbf{r}}$ is the excitation energy of site $\mathbf{r}$ which is equal to $\hbar\Omega$ when site $\mathbf{r}$ is occupied and is equal to ϵ_1 when site $\mathbf{r}$ is not occupied by molecules. Therefore $\epsilon_{\mathbf{r}}$ is a random variable with a binary probability distribution,[17]

$$p(\epsilon_{\mathbf{r}})=c\delta(\epsilon_{\mathbf{r}}-\hbar\Omega)+(1-c)\delta(\epsilon_{\mathbf{r}}-\epsilon_1). \tag{5}$$

By taking the $\epsilon_1\to\infty$ limit, we make the unoccupied sites inaccessible, and the Hamiltonian $H_{\rm ex}$ then represents our exciton system with topological disorder,[17]

$$\hat{\Gamma}=\sum_{\mathbf{r},\mathbf{r}'}\Gamma(\mathbf{r}-\mathbf{r}')B_{\mathbf{r}}^{+}B_{\mathbf{r}'}, \tag{6}$$

is the effective radiative damping operator. We have neglected the coupling between single exciton and two exciton states because we are only interested in the single exciton subspace. The $\mathbf{r}$ dependence of $J(\mathbf{r})$ and $\Gamma(\mathbf{r})$ will be specified later.

$H_{\rm int}$ denotes the exciton–field interaction. Adopting the interaction picture with respect to the radiation field Hamiltonian, the electric field operator is given by

$$E(\mathbf{r},t)=\mathbf{E}_1(t)e^{i(\kappa_1\cdot\mathbf{r}-\bar{\omega}_1t)}+\mathbf{E}_2e^{i(\kappa_2\cdot\mathbf{r}-\bar{\omega}_2t)}+\text{c.c.}, \tag{7}$$

where c.c. denote complex conjugate, E_1 and E_2 denote the incident and the scattered modes, respectively,

$$|\kappa_1|=\frac{\bar{\omega}_1}{c_0},\quad |\kappa_2|=\frac{\bar{\omega}_2}{c_0},$$

and c_0 is the speed of light. $\mathbf{E}_1(t)$ is a classical function of time, and $\mathbf{E}_2$ is a quantum operator

$$\mathbf{E}_2=c_2a_2\hat{e}_2, \tag{8a}$$

$$\mathbf{E}_2^{*}=c_2^{*}a_2^{+}\hat{e}_2, \tag{8b}$$

where a_2^{+}, a_2 are creation and annihilation operators of the scattered photon mode (κ_2,ω_2), which satisfy the Bose commutation relation $[a_2,a_2^{+}]=1$. $\hat{e}_2\perp\kappa_2$ is the polarization direction of the scattered mode, and

$$c_2=-i(2\pi\hbar\omega_2/V)^{1/2}, \tag{9}$$

with V being the quantization volume. Hereafter we take $\hbar=1$.

The exciton–field interaction is given by

$$\begin{aligned}H_{\rm int}=-\sum_{\mathbf{r}}(B_{\mathbf{r}}+B_{\mathbf{r}}^{+})\{&[\mathbf{E}_1(t)\cdot\boldsymbol{\mu}]e^{i(\kappa_1\cdot\mathbf{r}-\bar{\omega}_1t)}\\&+c_2(\hat{e}_2\cdot\boldsymbol{\mu})a_2\,e^{i(\kappa_2\cdot\mathbf{r}-\bar{\omega}_2t)}+[\mathbf{E}_1^{*}(t)\cdot\boldsymbol{\mu}]\\&\times e^{-i(\kappa_1\cdot\mathbf{r}-\bar{\omega}_1t)}+c_2^{*}(\hat{e}_2\cdot\boldsymbol{\mu})a_2^{+}e^{-i(\kappa_2\cdot\mathbf{r}-\bar{\omega}_2t)}\}.\end{aligned} \tag{10}$$

The time dependent emission rate of (κ_2,ω_2) photons is formally given by[23]

$$\begin{aligned}S(\kappa_1,\kappa_2,t)&=\left\langle\frac{d}{dt}a_2^{+}a_2\right\rangle\\&=i\langle[H_{\rm int},a_2^{+}a_2]\rangle\\&=-i\,\mathrm{Tr}\{a_2^{+}a_2\,[H_{\rm int},\rho(t)]\}.\end{aligned} \tag{11}$$

Here $\rho(t)$ is the density operator of the system (material and the scattered field mode), which satisfied the Liouville equation

$$\frac{d}{dt}\rho(t)=-i[H\rho(t)-\rho(t)H^{\dagger}]. \tag{12}$$

The total photon emission rate is

$$\sum_{\kappa_2} S(\kappa_1,\kappa_2,t) \rightarrow \frac{V}{(2\pi c_0)^3} \int d\Omega \int_0^{\omega_B} d\bar{\omega}_2 \bar{\omega}_2^2 S(\kappa_1,\kappa_2,t), \tag{13}$$

where Ω denotes the solid angle. The $\bar{\omega}_2$ integration should be cut off[24] at $\omega_B \sim 2\pi c_0/a_B$ (a_B is the Bohr radius) beyond which the dipole approximation breaks down. We are interested in the photon emission rate to the unit solid angle in direction $\hat{\kappa}_2$, $(dn/d\Omega)(\kappa_1,\hat{\kappa}_2,t)$,

$$\frac{dn}{d\Omega} \equiv \frac{V}{(2\pi c_0)^3} \int_0^{\omega_B} d\bar{\omega}_2 \bar{\omega}_2^2 S(\kappa_1,\kappa_2,t). \tag{14}$$

In Appendix A we derive the following Green's function expression for this rate

$$\frac{dn}{d\Omega} = \frac{\Omega^3}{8\pi^3 c_0^3} (\hat{e}_1 \cdot \boldsymbol{\mu})^2 (\hat{e}_2 \cdot \boldsymbol{\mu})^2 \sum_{\mathbf{r}_1,\mathbf{r}_2,\mathbf{r}_3,\mathbf{r}_4} \int d\omega_1 \times \int d\omega_2 \phi(\mathbf{r}_1,\mathbf{r}_2,\mathbf{r}_3,\mathbf{r}_4;\omega_1,\omega_2) \times e^{i\kappa_1 \cdot \mathbf{r}_{24}} e^{-i\kappa_2 \cdot \mathbf{r}_{13}} \tilde{E}(\omega_1) \tilde{E}^*(\omega_2) e^{-i\omega_{12} t}, \tag{15}$$

where $\mathbf{r}_{ij} = \mathbf{r}_i - \mathbf{r}_j$, $\omega_{12} = \omega_1 - \omega_2$, $\kappa_2 = (\Omega/c_0)\hat{\kappa}_2$, and $\tilde{E}(\omega)$ is the temporal Fourier transform of incoming pulse $E_1(t)$,

$$\tilde{E}(\omega) = \int_{-\infty}^{\infty} dt E_1(t) e^{i(\omega - \bar{\omega}_1)t}, \qquad E_1(t) = \frac{1}{2\pi} \int d\omega \tilde{E}(\omega) e^{i(\bar{\omega}_1 - \omega)t}. \tag{16}$$

ϕ is the configurationally averaged particle–hole (p–h) Green's function

$$\phi(\mathbf{r}_1,\mathbf{r}_2,\mathbf{r}_3,\mathbf{r}_4;\omega_1,\omega_2) \equiv \overline{G_{\mathbf{r}_1,\mathbf{r}_2}(\omega_1) G^*_{\mathbf{r}_3,\mathbf{r}_4}(\omega_2)}. \tag{17}$$

We use an overbar to denote the average over all configurations, and G is the single particle Green's function

$$G_{\mathbf{r},\mathbf{r}'}(\omega) = \langle \mathbf{r} | \frac{1}{\omega - H_{\text{eff}} + i0} | \mathbf{r}' \rangle. \tag{18}$$

Equation (15) can alternatively be recast in the form

$$\frac{dn}{d\Omega} = \frac{\Omega^3}{2\pi c_0^3} (\hat{e}_1 \cdot \boldsymbol{\mu})^2 (\hat{e}_2 \cdot \boldsymbol{\mu})^2 \overline{|P(\kappa_2,t)|^2}, \tag{19}$$

where $P(\kappa_2,t)$ is the optical polarization in k space

$$P(\kappa_2,t) = \sum_{\mathbf{r}} P(\mathbf{r},t) e^{-i\kappa_2 \cdot \mathbf{r}} = -\sum_{\mathbf{r},\mathbf{r}'} e^{-i\kappa_2 \cdot \mathbf{r}} \int \frac{d\omega}{2\pi} G_{\mathbf{r},\mathbf{r}'}(\omega) E(\omega) e^{i\kappa_1 \cdot \mathbf{r}' - i\omega t}. \tag{20}$$

III. LADDER DIAGRAM APPROXIMATION FOR THE GREEN FUNCTION IN TWO DIMENSIONS

In the previous section, we expressed the fluorescence of a molecular assembly in terms of p–h Green functions [see Eq. (15)]. For a two-dimensional monolayer, we have

$$\frac{dn}{d\Omega} = M \frac{\Omega^3}{8\pi^3 c_0^3} (\hat{e}_1 \cdot \boldsymbol{\mu})^2 (\hat{e}_2 \cdot \boldsymbol{\mu})^2 \int d\omega_1 \int d\omega_2 \times \phi(\mathbf{k}_2,\mathbf{k}_1,\mathbf{q}=0;\omega_1,\omega_2) \tilde{E}(\omega_1) \tilde{E}^*(\omega_2) e^{-i\omega_{12} t}, \tag{21}$$

where $\mathbf{k}_1$, $\mathbf{k}_2$ are the projections of κ_1, κ_2 in the monolayer plane, and $\phi(\mathbf{p},\mathbf{p}',\mathbf{q};\omega_1,\omega_2)$ is the p–h Green function in momentum space

$$\phi(\mathbf{p},\mathbf{p}',\mathbf{q};\omega_1,\omega_2) \equiv \frac{1}{M} \sum_{\mathbf{r}_1,\mathbf{r}_2,\mathbf{r}_3,\mathbf{r}_4} \phi(\mathbf{r}_1,\mathbf{r}_2,\mathbf{r}_3,\mathbf{r}_4;\omega_1,\omega_2) \times \exp[-i(\mathbf{p}+\mathbf{q}/2)\cdot\mathbf{r}_1 + i(\mathbf{p}'+\mathbf{q}/2)\cdot\mathbf{r}_2 + i(\mathbf{p}-\mathbf{q}/2)\cdot\mathbf{r}_3 - i(\mathbf{p}'-\mathbf{q}/2)\cdot\mathbf{r}_4]. \tag{22}$$

We have recently developed a procedure for calculating the Green's function for a topologically disordered infinite lattice based on the ladder diagram approximation.[17] We assume that the aggregate size is large compared with the effective coherence size for cooperative emission, so that boundary effects are negligible, and we can assume translational invariance and apply the method of Ref. 17. We can check for consistency by comparing the coherence size calculated by this method with the aggregate size.

We define the configurationally averaged single particle Green function $G(\mathbf{p},\omega)$ in momentum space as

$$G(\mathbf{p},\omega) = \sum_{\mathbf{r}-\mathbf{r}'} G(\mathbf{r}-\mathbf{r}',\omega) e^{-i\mathbf{p}\cdot(\mathbf{r}-\mathbf{r}')}, \tag{23a}$$

$$G(\mathbf{r}-\mathbf{r}',\omega) = \overline{\hat{G}_{\mathbf{r},\mathbf{r}'}(\omega)}. \tag{23b}$$

In Appendix B we show that the photon emission rate can be separated into a coherent component S_c,

$$S_c = \int d\omega_1 \int d\omega_2 G(\mathbf{k}_1,\omega_1) G^*(\mathbf{k}_1,\omega_2) \tilde{E}(\omega_1) \times \tilde{E}^*(\omega_2) e^{-i\omega_{12} t} = \left| \int d\omega_1 G(\mathbf{k}_1,\omega_1) \tilde{E}(\omega_1) e^{-i\omega_1 t} \right|^2, \tag{24}$$

and an incoherent component S_I,

$$S_I=\int d\omega_1 \int d\omega_2 G(\mathbf{k}_2,\omega_1)G^*(\mathbf{k}_2,\omega_2)G(\mathbf{k}_1,\omega_1)G^*(\mathbf{k}_1,\omega_2)$$

$$\times\frac{G(\omega_1)-G^*(\omega_2)-[\omega_{21}-i\Gamma_{12}(\omega_1,\omega_2)]L(\mathbf{q}=0;\omega_1,\omega_2)}{[\omega_{21}-i\Gamma_{12}(\omega_1,\omega_2)]L^2(\mathbf{q}=0;\omega_1,\omega_2)}\tilde{E}(\omega_1)\tilde{E}^*(\omega_2)e^{-i\omega_{12}t}. \tag{25}$$

The total signal is

$$\frac{dn}{d\Omega}=\frac{\Omega^3}{8\pi^3 c_0^3}(\hat{e}_1\cdot\mu)^2(\hat{e}_2\cdot\mu)^2\,[M^2S_c\Delta(\mathbf{k}_1-\mathbf{k}_2)+MS_I]. \tag{26}$$

We have further defined

$$L(\mathbf{q};\omega_1,\omega_2)\equiv\frac{1}{M}\sum_{\mathbf{p}}G(\mathbf{p}+\mathbf{q}/2,\omega_1)G^*(\mathbf{p}-\mathbf{q}/2,\omega_2), \tag{27}$$

$$\Gamma_{12}(\omega_1,\omega_2)=\frac{2\Sigma_{\mathbf{p}}\Gamma(\mathbf{p})G(\mathbf{p},\omega_1)G^*(\mathbf{p},\omega_2)}{\Sigma_{\mathbf{p}}G(\mathbf{p},\omega_1)G^*(\mathbf{p},\omega_2)}, \tag{28}$$

$$G(\omega)=\frac{1}{M}\sum_{\mathbf{p}}G(\mathbf{p},\omega). \tag{29}$$

Here $\Gamma(\mathbf{p})$ is the spatial Fourier transform of $\Gamma(\mathbf{r})$,

$$\Gamma(\mathbf{p})=\sum_{\mathbf{r}}\Gamma(\mathbf{r})e^{-i\mathbf{p}\cdot\mathbf{r}}. \tag{30}$$

$\Delta(\mathbf{k})$ is defined as

$$\Delta(\mathbf{k})=\frac{1}{M}\sum_{\mathbf{r}}e^{i\mathbf{k}\cdot\mathbf{r}}. \tag{31}$$

When the lattice size is much smaller than the optical wavelength, $\Delta(\mathbf{k}_1-\mathbf{k}_2)=1$, and the signal S_c is observed in all directions. On the other hand, when the lattice size is much larger than the optical wavelength, $\Delta(\mathbf{k}_1-\mathbf{k}_2)$ is nonzero only when $\mathbf{k}_2\simeq\mathbf{k}_1$, and the S_c signal is highly directional.

The coherent component S_c in Eq. (26) can be obtained by factorizing the p–h Green function ($\phi = \overline{GG} = \bar{G}\bar{G}$). Its contribution to the signal is proportional to M^2, and it decays in a time scale τ_0 which is determined by the longer of the two times, D^{-1}, the inverse spectral width of the Green's function $G(\mathbf{k}_2,\omega)$, or W^{-1}, the inverse spectral width of the excitation pulse (i.e., the pulse duration). The contribution of the incoherent component S_I to the signal is proportional to M. When Γ_{12} is much smaller than D and W, i.e., the radiative decay rate is much smaller than the absorption and excitation pulse linewidth, S_I decays in the radiative time scale $\Gamma_{12}^{-1}(\bar{\omega}_1,\bar{\omega}_1)$. Under this condition, we can obtain the long time behavior of S_I by setting $\omega_2=\omega_1$ everywhere except $\omega_{21}-i\Gamma_{12}(\omega_1,\omega_1)$ in the denominator. We thus have

$$S_I\simeq 4\pi^2 c\int d\omega A(\omega)\gamma(\omega)e^{-\gamma(\omega)t}|\tilde{E}(\omega)|^2, \tag{32}$$

where

$$\gamma(\omega)=\Gamma_{12}(\omega,\omega)=\frac{2\Sigma_{\mathbf{p}}|G(\mathbf{p},\omega)|^2\Gamma(\mathbf{p})}{\Sigma_{\mathbf{p}}|G(\mathbf{p},\omega)|^2} \tag{33}$$

is the average radiative decay rate of eigenstates with energy ω, and

$$A(\omega)=-\frac{1}{\pi c}|G(\mathbf{k}_2,\omega)|^2|G(\mathbf{k}_1,\omega)|^2$$

$$\times\frac{[\mathrm{Im}\,G(\omega)+\gamma(\omega)L(\mathbf{q}=0;\omega,\omega)/2]}{L^2(\mathbf{q}=0;\omega,\omega)\gamma(\omega)}. \tag{34}$$

Equation (32) represents the coarsed grained solution[1] which applies as long as the radiative lifetime is much longer than D^{-1} and W^{-1}, thus the signal approaches its long time behavior immediately. This is verified by our numerical calculations.

Equations (26), (24), and (32) express the time resolved fluorescence in terms of the single particle Green function. To complete the derivation we need an explicit expression for this Green function. This can be derived using the coherent potential approximation (CPA).[17] We then have

$$G(\mathbf{p},\omega)=\frac{1}{\omega-\Omega-\Sigma(\omega)-J(\mathbf{p})+i\Gamma(\mathbf{p})+i0}, \tag{35}$$

where $J(\mathbf{p})$ is the spatial Fourier transform of $J(\mathbf{r})$,

$$J(\mathbf{p})=\sum_{\mathbf{r}\neq 0}J(\mathbf{r})e^{-i\mathbf{p}\cdot\mathbf{r}}. \tag{36}$$

The self-energy $\Sigma(\omega)$ is determined by the self-consistent equation

$$\frac{1}{M}\sum_{\mathbf{p}}\frac{1}{\omega-\Omega-\Sigma(\omega)-J(\mathbf{p})+i\Gamma(\mathbf{p})+i0}=\frac{(c-1)}{\Sigma(\omega)}. \tag{37}$$

In summary, the present procedure for calculating the fluorescence consists of the following steps: (i) Solve the self-consistent Eq. (37) for $\Sigma(\omega)$. (ii) Substitute into Eqs. (35), (29), and (27) to determine $G(\mathbf{p},\omega)$, $G(\omega)$, and $L(\mathbf{q}=0;\omega_1,\omega_2)$. (iii) Substitute into Eqs. (33) and (34) to get $\gamma(\omega)$ and $A(\omega)$. (iv) Substitute into Eqs. (24) and (32) to get S_c and S_I. (v) Substitute into Eq. (26) to obtain the signal.

IV. APPLICATION TO SMALL TWO-DIMENSIONAL AGGREGATES

Up to this point, we have only assumed that the aggregate size is larger than the coherence size. We now further assume that the aggregate is much smaller than the optical wavelength of excitation, so that[2]

$$\Gamma(\mathbf{r}-\mathbf{r}')=\frac{\gamma}{2}, \tag{38a}$$

$$\Gamma(\mathbf{p})=\frac{M\gamma}{2}\delta_{\mathbf{p},0}, \tag{38b}$$

where γ is the single molecule radiative decay rate

$$\gamma=\frac{4\mu^2\Omega^3}{3c_0^3}. \tag{39}$$

Substituting Eq. (38) into Eq. (33) and using Eq. (35), we obtain

$$\gamma(\omega)=\gamma N_{\text{eff}}(\omega), \tag{40}$$

where $N_{\text{eff}}(\omega)$, defined by this equation, is the effective coherence size at a given energy ω,

$$N_{\text{eff}}(\omega)=\frac{1}{1+\alpha(\omega)}\cdot\frac{I(\omega)}{\rho(\omega)}. \tag{41}$$

Here

$$\alpha(\omega)=-\frac{\gamma}{2\,\text{Im}\,G(\omega)}\sum_{\mathbf{p}\neq 0}|G(\mathbf{p},\omega)|^2>0, \tag{42}$$

$\rho(\omega)$ is the single exciton density of states

$$\rho(\omega)=-\frac{1}{\pi c}\,\text{Im}\,G(\omega), \tag{43}$$

and $I(\omega)$ is the normalized linear absorption line shape $[\int d\omega I(\omega)=1]$,

$$I(\omega)=-\frac{1}{\pi c}\,\text{Im}\,G(\mathbf{p}=0,\omega). \tag{44}$$

Substituting Eqs. (27) and (40) into Eq. (34) and using Eqs. (35) and (37), and setting $\mathbf{k}_1=\mathbf{k}_2=0$, we have

$$A(\omega)=-\text{Im}\,\Sigma(\omega)\,|G(\mathbf{p}=0,\omega)|^2/(\pi c\gamma). \tag{45}$$

In deriving this equation, we have used the identity

$$\text{Im}\,G(\omega)=\text{Im}\,\Sigma(\omega)L(\mathbf{q}=0;\omega,\omega)-\frac{\gamma}{2}|G(\mathbf{p}=\mathbf{0},\omega)|^2, \tag{46}$$

which is obtained by substituting Eq. (35) into Eq. (29) and taking the imaginary part of both sides.

When c is not close to 1, and for ω within the band, the superradiance decay rate is much smaller than the inhomogeneous broadening

$$M\gamma/2\ll|\text{Im}\,\Sigma(\omega)|, \tag{47}$$

and we have from Eq. (35)

$$\text{Im}\,G(\mathbf{p},\omega)=\left[\text{Im}\,\Sigma(\omega)-\frac{M\gamma}{2}\delta_{\mathbf{p},0}\right]|G(\mathbf{p},\omega)|^2$$

$$\simeq\text{Im}\,\Sigma(\omega)\,|G(\mathbf{p},\omega)|^2. \tag{48}$$

Substituting this into Eq. (42), we have

$$\alpha(\omega)\ll 1, \tag{49}$$

and therefore

$$N_{\text{eff}}(\omega)=\frac{I(\omega)}{\rho(\omega)}, \tag{50}$$

$$A(\omega)=I(\omega)/\gamma, \tag{51}$$

Eq. (50) can be rationalized by a simple physical argument. Since the radiative decay rate of an eigenstate is proportional to its oscillator strength, and the linear absorption is equal to the density of states multiplied by the oscillator strength, the average radiative decay rate should be proportional to the absorption divided by the density of states. In the present formulation, both the absorption and the density of states are expressed in terms of the single particle Green function. However the average emission signal related to the average particle–hole Green function $\overline{GG}$ is not generally equal to the signal with the average decay rate. Making the factorization approximation $\overline{GG}=\bar{G}\bar{G}$, the incoherent signal vanishes. In the ladder diagram approximation and when the inhomogeneous broadening is larger than the superradiance decay rate [see Eq. (47)], Eq. (50) holds which implies that the decay rate of the average signal is equal to the average decay rate.

On the other hand, when $M\gamma/2\gg|\text{Im}\,\Sigma(\omega)|$, $\alpha(\omega)\gg 1$, and $N_{\text{eff}}(\omega)$ is much smaller than the average oscillator strength. The reason is as follows: The oscillator strength is proportional to the size within which the optical polarization of the various molecules oscillates in phase. This size is equal to $v(\omega)/\text{Im}\,\Sigma(w)$, where $v(\omega)$ is the exciton group velocity and $\text{Im}\,\Sigma(w)$ is the inverse dephasing time of exciton. When $M\gamma/2\gg|\text{Im}\,\Sigma(\omega)|$, the exciton moves in a region much smaller than $v(\omega)/\text{Im}\,\Sigma(w)$ during the super-radiance lifetime $1/M\gamma$. Therefore the number of molecules which can emit cooperatively, $N_{\text{eff}}(\omega)$, is much smaller than the average oscillator strength. For example in the regular lattice limit ($c\to 1$), the self-energy $\Sigma(\omega)\to 0$. When ω is close (but not exactly equal) to the energy of one of the eigenstates $J(\mathbf{p}\neq 0)$, we have from Eq. (42)

$$\alpha(\omega)\simeq|w-J(\mathbf{p}=0)+iM\gamma/2|^2/|w-J(\mathbf{p})|^2\gg 1, \tag{52}$$

and Eq. (50) breaks down. In fact Eq. (50) gives $N_{\text{eff}}(\omega)=M$ for all ω except $\omega=J(\mathbf{p}\neq 0)$ with $\mathbf{p}$ in the first Brillouin zone. This is clearly unphysical and we should use the more general expression Eq. (41) in which the correction factor $\alpha(\omega)$ is taken into account.

V. NUMERICAL RESULTS

In the following numerical calculations we modeled the aggregate as a square lattice with unit cell vectors $a\hat{x}$ and $a\hat{y}$. The transition dipole $\boldsymbol{\mu}$ is taken to be in the plane of the aggregate,

$$\boldsymbol{\mu}=\frac{\mu}{\sqrt{2}}(\hat{x}+\hat{y}).$$

We further assume nearest-neighbor interactions, so that

$$J(\mathbf{p})=-\frac{B}{2}[\cos(p_x a)+\cos(p_y a)]. \tag{53}$$

Here $2B$ is the bandwidth of a regular lattice ($c=1$),

$$B=\frac{2\mu^2}{a^3}. \tag{54}$$

For the present geometry the nearest-neighbor interaction is negative (J-aggregate). Condition (47) holds for frequencies ω inside the band, provided c is not too close to 1. We therefore neglect $\Gamma(\mathbf{p})$ in $G(\mathbf{p},\omega)$. From Eq. (37), we have

$$\Sigma(\omega)\int d\epsilon\frac{\rho_0(\epsilon)}{\omega-\Sigma(\omega)-\epsilon+i0}=c-1, \tag{55}$$

where $\rho_0(\epsilon)$ is the density of states of regular lattice ($c=1$),

$$\rho_0(\epsilon)=\frac{1}{M}\sum_{\mathbf{p}}\delta[\epsilon-\Omega-J(\mathbf{p})]. \tag{56}$$

We shall approximate $\rho_0(\epsilon)$ by a simple Hubbard form which retains the correct analytic behavior near the band edges, and has no singularity within the band and gives one state per site,[27]

$$\rho_0(\epsilon)=\begin{cases}\dfrac{1}{2B} & |\epsilon-\Omega|<B\\ 0 & |\epsilon-\Omega|>B.\end{cases} \tag{57}$$

Substituting this into Eq. (55), we get

$$\frac{\Sigma(\omega)}{2B}\ln\frac{\omega-\Omega-\Sigma(\omega)+B}{\omega-\Omega-\Sigma(\omega)-B}=c-1. \tag{58}$$

We have solved Eq. (58) for $\Sigma(\omega)$ numerically by calculating the complex root for a given ω using Newton's method.[28] From Eq. (50) we obtain the coherence size as a function of energy ω. The results are displayed in Fig. 1. The figure shows that the coherence size attains its maximum value at the bottom of the band, which carries most of the oscillator strength. This is characteristic of J-aggregates. For a regular lattice ($c=1$) with periodic boundary conditions, the $\mathbf{k}=0$ state which carries all the oscillator strength is at the bottom of the band [see Eq. (53)]. When $c<1$, the oscillator strength is distributed among states near the band edge. The figure also shows that as the disorder increases (c decreases), the distribution of oscillator strength becomes broader, and the maximum coherence size decreases. We display the maximum coherence size across the band N_c as a function of density c in Fig. 2. The figure demonstrates that when the disorder increases (c decreases), N_c decreases. The disorder thus destroys the cooperativity of the aggregate. In the low density ($c\to 0$) limit, $N_c\to 1$, which means that each molecule radiates independently. From the figure we also see that as $c\to 1$, $N_c\to\infty$. However the present theory only holds when

$$N_c<N=cM\ll c(\lambda/a)^2. \tag{59}$$

As N increases for a given density c, the maximum coherence size first increases linearly with N and then converges to some asymptotic limiting value N_c (Ref. 1) which is determined by the density c and is independent of N as long as λ is much larger than the aggregate size.

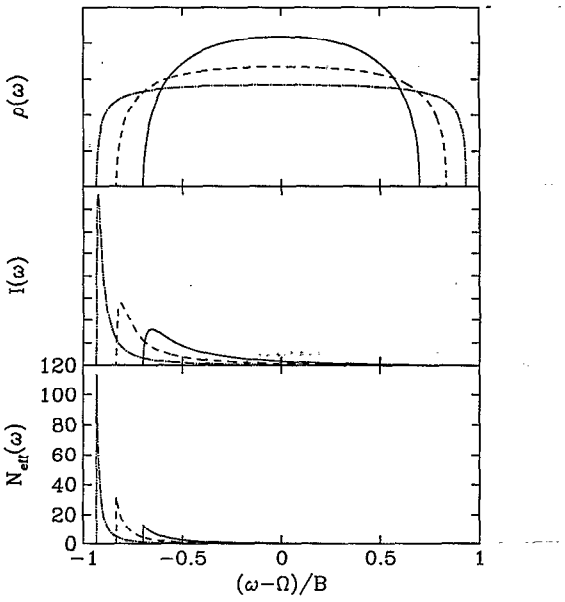

FIG. 1. Molecular density of states, absorption line shape, and coherence size as a function of energy for three different densities. Solid line $c=0.4$, dashed line $c=0.6$, and dash–dotted line $c=0.8$. Note that the coherence size is only defined within the band. The vertical lines in the lowest panel denote the band edge.

If relaxation among the various exciton states in the band is negligible, $N_{\text{eff}}(\omega)$ can be measured experimently by applying a pulse whose spectral width W is much narrower than the inhomogeneous broadening of single exciton states and is much larger than the radiative decay rate, i.e.,

$$|\operatorname{Im}\Sigma(\bar{\omega}_1)|\gg W\gg\gamma(\bar{\omega}_1).$$

From Eqs. (24) and (32) we have in this case

$$S_c\simeq 4\pi^2|G(\mathbf{k}_1,\bar{\omega}_1)|^2|E_1(t)|^2, \tag{60a}$$

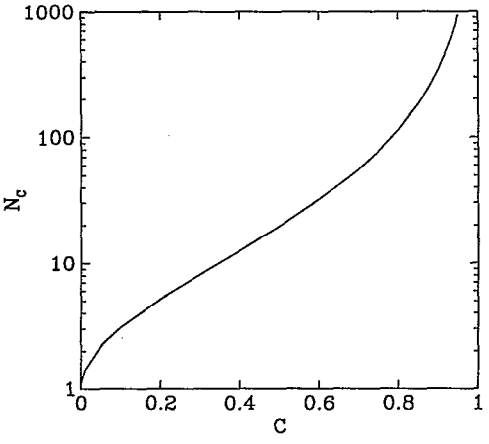

FIG. 2. Maximum coherence size N_c as a function of molecular density c plotted on a logarithmic scale.

$$S_I \simeq 8\pi^3 cA(\bar{\omega}_1)\gamma(\bar{\omega}_1)e^{-\gamma(\bar{\omega}_1)t}\int dt' |E_1(t')|^2. \quad (60b)$$

Here $\bar{\omega}_1$ is the peak position of the incoming pulse $\tilde{E}(\omega_1)$. Since $W \gg \gamma(\bar{\omega}_1)$, we see from Eq. (60) that S_c decays much faster than S_I. After a short time delay (which is equal to the duration of the incoming pulse), the signal then decays exponentially. This allows us to measure the energy dependent radiative decay rate $\gamma(\bar{\omega}_1)$ and coherence size $N_{\text{eff}}(\bar{\omega}_1)$. In practice, neglect of relaxation among the exciton states is only likely to be realistic for very low temperatures and relatively short times. As relaxation occurs, emission will tend to be dominantly from lowest states in the band and the information on the dependence of N_{eff} on $\bar{\omega}_1$ may not be readily observable.

When the incoming pulse is very short (impulsive excitation), $E_1(t)=E_1\delta(t)$ or $\tilde{E}_1(\omega)=E_1=\text{const}$, we have from Eq. (24),

$$S_c = \left| \int d\omega_1 G(\mathbf{k}_1,\omega_1)e^{-i\omega_1 t}\right|^2 |E_1|^2. \quad (61)$$

Since

$$\int d\omega_1 G^*(\mathbf{k}_1,\omega_1)e^{-i\omega_1 t}=0 \quad t>0, \quad (62)$$

we have

$$S_c = 4\pi^2 c^2 \left| \int d\omega_1 I(\omega_1)e^{-i\omega_1 t}\right|^2 |E_1|^2 \quad t>0. \quad (63)$$

Here $I(\omega_1)$ is the absorption line shape defined in Eq. (44), and we have set $\mathbf{k}_1=0$. The above equation shows that the coherent component $S_c(t)$ is simply given by the square of the Fourier transform of the absorption line shape. S_c decays due to inhomogeneous dephasing (free induction decay) in a time scale equal to the inverse of the absorption linewidth which is much shorter than the radiative lifetime $1/\gamma(\bar{\omega}_1)$ when c is not too large. S_I has a multiexponential decay in the impulsive excitation case [see Eq. (32)]. $S_c(t)$ and $S_I(t)$ calculated for impulsive excitation are displayed in Figs. 3 and 4. These figures demonstrate that S_c decays much faster than S_I.

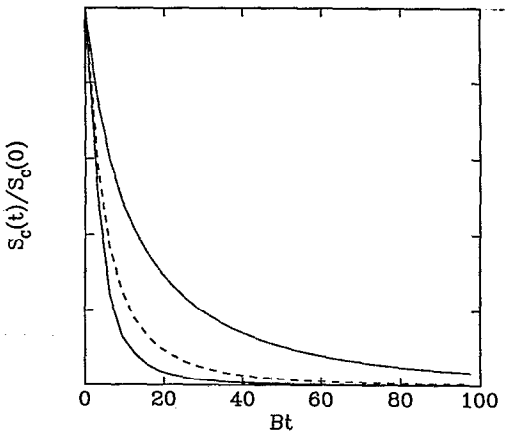

FIG. 3. The coherent emission $S_c(t)$ [normalized to $S_c(0)$] as a function of time t following an impulsive excitation for three different densities. Solid line $c=0.4$, dashed line $c=0.6$, and dash–dotted line $c=0.8$. The ratio of $S_c(0)$ for the three curves is 1 : 2.25 : 4.0.

VI. DISCUSSION

We have investigated the radiative dynamics of molecular aggregates with topological disorder. The photon emission rate was expressed in terms of a configurationally averaged p–h Green's function [see Eq. (21)], and then evaluated it using the ladder diagram approximation. We found that following an initial short time decay [$S_c(t)$], the signal is characterized by a cooperative radiative decay [$S_I(t)$]. The energy dependent coherence size and the maximum coherence size for different densities were calculated. The signal was analyzed using two limiting cases for the excitation pulses. (i) The pulse spectral width is much smaller than the inhomogeneous broadening but much larger than the radiative decay rate. (ii) Infinitely short pulse (impulsive) excitation.

Although we have assumed $\text{Im}\,\Sigma(\omega) \gg M\gamma/2$ for ω within the band in our numerical calculations, this is not a fundamental limitation of our theory. When this condition does not hold, we should solve the CPA self-consistent Eq. (37) instead of Eq. (55), and use Eqs. (41), (45) to calculate $N_{\text{eff}}(\omega)$, $A(\omega)$ instead of using Eqs. (50), (51). Moreover, our two-dimensional numerical calculations can be easily extended to one- or three-dimensional aggregates whose size is much smaller than the optical wavelength. Our theory can also be applied to infinite superlattices and nanostructures.[4–6,29] Considering an infinite two-dimensional lattice, Eqs. (26) and (31) show that S_c is highly directional and can be observed only in the direction $\mathbf{k}_2 \simeq \mathbf{k}_1$, while S_I can be observed in all directions. Equation (38) does not hold. $\Gamma(\mathbf{r})$ is given by[2,24]

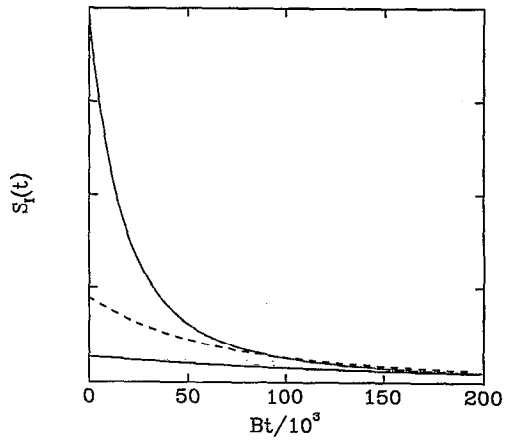

FIG. 4. The incoherent emission S_I as a function of time t following an impulsive excitation for three different densities. Solid line $c=0.4$, dashed line $c=0.6$, and dash–dotted line $c=0.8$.

$$\Gamma(\mathbf{r})=\frac{3}{4}\gamma\left\{(1-\cos^2\theta)\frac{\sin(kr)}{kr}+(1-3\cos^2\theta)\times\left[\frac{\cos(kr)}{(kr)^2}-\frac{\sin(kr)}{(kr)^3}\right]\right\}. \quad (64)$$

Here $k=\Omega/c_0$, θ is the angle between $\boldsymbol{\mu}$ and $\mathbf{r}$. The energy dependent decay rate $\gamma(\omega)$ should be calculated from Eq. (33) rather than Eq. (40).

For a regular infinite lattice ($c=1$), $S_I=0$ and the signal shows up only in the direction $\mathbf{k}_2=\mathbf{k}_1$. For impulsive excitation, the signal decays as

$$e^{-2\Gamma(\mathbf{k}_1)t},$$

which agrees with the result of Jenkins and Mukamel.[5] Choosing $\mathbf{k}_1=0$, we have[5,30]

$$\Gamma(\mathbf{k}_1=0)=\frac{3\pi}{2}\gamma\left(\frac{\tilde{\lambda}}{a}\right)^2, \quad (65)$$

where $\tilde{\lambda}=c_0/\Omega$. The extension of these results to one-dimensional infinite lattices is straightforward. A three-dimensional infinite lattice is radiatively stable.[30,31] Allowing for retarded interactions in such crystals leads to polariton waves, which have no radiative damping.[29–32] In order to retain polariton effects,[29,33,34] Eq. (64) needs to be modified to account for the retarded (i.e., nonlocal in time) nature of the interaction by incorporating its frequency dependence.

ACKNOWLEDGMENT

The support of the National Science Foundation Center for Photoinduced Charge Transfer is gratefully acknowledged.

APPENDIX A

In this Appendix we derive Eq. (15) by extending the approach of Ref. 23. Starting from Eq. (11) and expanding $\rho(t)$ to the third order of $H_{\rm int}$, we have

$$S(\mathbf{k}_1,\mathbf{k}_2,t)=\int_0^\infty dt_1\int_0^\infty dt_2\int_0^\infty dt_3 \times\mathrm{Tr}[a_2^+a_2L_{\rm int}(t)\mathscr{G}(t_3)L_{\rm int}(t-t_3)\times\mathscr{G}(t_2)L_{\rm int}(t-t_2-t_3)\mathscr{G}(t_1)\times L_{\rm int}(t-t_1-t_2-t_3)\rho(-\infty)]. \quad (A1)$$

Here $\rho(-\infty)=|00\rangle\langle 00|$ with $|00\rangle$ denotes the vacuum state (no exciton and scattered photon). The action of Liouville space operators $L_{\rm int}(t)$ and $\mathscr{G}(t)$ on any given operator A is defined by

$$L_{\rm int}(t)A\equiv[H_{\rm int}(t),A], \quad (A2)$$
$$\mathscr{G}(t)A\equiv e^{-iH_{\rm eff}t}Ae^{iH_{\rm eff}^+t}.$$

From Eq. (A1) we see that the system interacts with $H_{\rm int}$ four times. In the first three interactions, $H_{\rm int}$ can act either from the left or from the right. Whether $H_{\rm int}$ acts from the left or from the right in the fourth interaction is uniquely determined by the first three interactions. In the first three interactions, the system can interact with either the external field E_1 or the scattered field E_2, while the fourth interaction must be E_2, otherwise the trace is zero. This results in 64 terms. In the rotating wave approximation, the number of resonant terms is greatly reduced. For example, the first interaction must be with E_1 to create an exciton. Terms such as $B_{\mathbf{r}}^+a_2^+e^{i\bar{\omega}_2t}$, $B_{\mathbf{r}}^+E_1^*(t)e^{i\bar{\omega}_1t}$ which represent the creation of an exciton and emission of a photon are antiresonant and are thus omitted. We find that only six terms survive. The contribution of three of them are the complex conjugate of the others. So in practice we need to consider only three pathways (see Fig. 8 of Ref. 23). We then get[23,35]

$$S(\boldsymbol{\kappa}_1,\boldsymbol{\kappa}_2,t)=(\hat{e}_1\cdot\boldsymbol{\mu})^2(\hat{e}_2\cdot\boldsymbol{\mu})^2|c_2|^2(\mathrm{I}+\mathrm{II}+\mathrm{III})+\mathrm{c.c.}, \quad (A3)$$

where

$$\mathrm{I}=\sum_{\mathbf{r}_1,\mathbf{r}_2,\mathbf{r}_3,\mathbf{r}_4}\int_0^\infty dt_1\int_0^\infty dt_2\int_0^\infty dt_3\,e^{-i\bar{\omega}_1t_1}e^{-i\bar{\omega}_2t_3}\times e^{i\boldsymbol{\kappa}_1\cdot\mathbf{r}_{34}}e^{i\boldsymbol{\kappa}_2\cdot\mathbf{r}_{12}}E_1^*(t-t_1-t_2-t_3)E_1(t-t_2-t_3)\times\langle\mathbf{r}_2|e^{-iH_{\rm eff}t_2}|\mathbf{r}_3\rangle\langle\mathbf{r}_4|e^{iH_{\rm eff}^+(t_1+t_2+t_3)}|\mathbf{r}_1\rangle, \quad (A4a)$$

$$\mathrm{II}=\sum_{\mathbf{r}_1,\mathbf{r}_2,\mathbf{r}_3,\mathbf{r}_4}\int_0^\infty dt_1\int_0^\infty dt_2\int_0^\infty dt_3\,e^{-i\bar{\omega}_1t_1}e^{i\bar{\omega}_2t_3}\times e^{i\boldsymbol{\kappa}_1\cdot\mathbf{r}_{34}}e^{i\boldsymbol{\kappa}_2\cdot\mathbf{r}_{21}}E_1^*(t-t_1-t_2-t_3)E_1(t-t_2-t_3)\times\langle\mathbf{r}_1|e^{-iH_{\rm eff}(t_2+t_3)}|\mathbf{r}_3\rangle\langle\mathbf{r}_4|e^{iH_{\rm eff}^+(t_1+t_2)}|\mathbf{r}_2\rangle, \quad (A4b)$$

$$\mathrm{III}=\sum_{\mathbf{r}_1,\mathbf{r}_2,\mathbf{r}_3,\mathbf{r}_4}\int_0^\infty dt_1\int_0^\infty dt_2\int_0^\infty dt_3e^{-i\bar{\omega}_1t_1}\times e^{-i(\bar{\omega}_1-\bar{\omega}_2)t_2}e^{i\bar{\omega}_2t_3}e^{i\boldsymbol{\kappa}_1\cdot\mathbf{r}_{24}}e^{i\boldsymbol{\kappa}_2\cdot\mathbf{r}_{31}}E_1^*(t-t_1-t_2-t_3)\times E_1(t-t_3)\langle\mathbf{r}_1|e^{-iH_{\rm eff}t_3}|\mathbf{r}_2\rangle\langle\mathbf{r}_4|e^{iH_{\rm eff}^+t_1}|\mathbf{r}_3\rangle. \quad (A4c)$$

Here $\mathbf{r}_{ij}=\mathbf{r}_i-\mathbf{r}_j$, and I, II, III corresponds to the three pathways shown in Fig. 8 of Ref. 23.

Substituting Eq. (A3) into Eq. (14) and setting $\hbar=1$, we have

$$\frac{dn}{d\Omega}=\frac{1}{4\pi^2c_0^3}(\hat{e}_1\cdot\boldsymbol{\mu})^2(\hat{e}_2\cdot\boldsymbol{\mu})^2\times\int_0^{\omega_B}d\bar{\omega}_2\bar{\omega}_2^3(\mathrm{I}+\mathrm{II}+\mathrm{III})+\mathrm{c.c.} \quad (A5)$$

Since I, II, and III are resonant at $\bar{\omega}_2=\Omega$, we can replace the $\bar{\omega}_2^3$ factor by Ω^3 and take it out of the integration, then setting $\kappa_2=\Omega/c_0$ and extend the range of $\bar{\omega}_2$ integration to $\int_{-\infty}^{\infty}$. The $\bar{\omega}_2$ integration in III gives $\delta(t_2+t_3)$ which gives zero when the t_2 and t_3 integrations are performed. The $\bar{\omega}_2$ integration in I and II both give $\delta(t_3)$. Interchanging $\mathbf{r}_1$, $\mathbf{r}_2$ in II, we see that the contribution to $dn/d\Omega$ from II is the same as I. We finally have

$$\frac{dn}{d\Omega}=\frac{\Omega^3}{4\pi^2c_0^3}(\hat{e}_1\cdot\boldsymbol{\mu})^2(\hat{e}_2\cdot\boldsymbol{\mu})^2\cdot 2\pi\sum_{\mathbf{r}_1,\mathbf{r}_2,\mathbf{r}_3,\mathbf{r}_4}\int_0^\infty dt_1$$
$$\times\int_0^\infty dt_2 e^{-i\bar{\omega}_1 t_1}e^{i\kappa_1\cdot\mathbf{r}_{34}}e^{i\Omega\hat{k}_2\cdot\mathbf{r}_{12}/c_0}$$
$$\times E_1^*(t-t_1-t_2)E_1(t-t_2)\langle\mathbf{r}_2|e^{-iH_{\rm eff}t_2}|\mathbf{r}_3\rangle$$
$$\times\langle\mathbf{r}_4|e^{iH_{\rm eff}^+(t_1+t_2)}|\mathbf{r}_1\rangle+\text{c.c.} \tag{A6}$$

Substituting Eq. (16) into Eq. (A6) and using the identities

$$e^{-iH_{\rm eff}t}=-\frac{1}{2\pi i}\int dE_1'\frac{e^{-iE_1't}}{E_1'-H_{\rm eff}+i0},$$
$$e^{iH_{\rm eff}^+t}=\frac{1}{2\pi i}\int dE_2'\frac{e^{iE_2't}}{E_2'-H_{\rm eff}^+-i0}, \tag{A7}$$

we have

$$\frac{dn}{d\Omega}=\frac{\Omega^3}{32\pi^5c_0^3}(\hat{e}_1\cdot\boldsymbol{\mu})^2(\hat{e}_2\cdot\boldsymbol{\mu})^2\sum_{\mathbf{r}_1,\mathbf{r}_2,\mathbf{r}_3,\mathbf{r}_4}\int_0^\infty dt_1\int_0^\infty dt_2\int dE_1'\int dE_2'\int d\omega_1\int d\omega_2\, e^{i\kappa_1\cdot\mathbf{r}_{34}}e^{i\Omega\hat{k}_2\cdot\mathbf{r}_{12}/c_0}$$
$$\times G_{\mathbf{r}_2,\mathbf{r}_3}(E_1')G^*_{\mathbf{r}_1,\mathbf{r}_4}(E_2')\tilde{E}(\omega_1)\tilde{E}^*(\omega_2)e^{i(E_2'-\omega_2)t_1}e^{i(E_{21}'+\omega_{12})t_2}e^{-i\omega_{12}t}+\text{c.c.}$$
$$=\frac{i\Omega^3}{16\pi^4c_0^3}(\hat{e}_1\cdot\boldsymbol{\mu})^2(\hat{e}_2\cdot\boldsymbol{\mu})^2\sum_{\mathbf{r}_1,\mathbf{r}_2,\mathbf{r}_3,\mathbf{r}_4}\int dE_2'\int d\omega_1\int d\omega_2 e^{i\kappa_1\cdot\mathbf{r}_{34}}e^{i\Omega\hat{k}_2\cdot\mathbf{r}_{12}/c_0}$$
$$\times G_{\mathbf{r}_2,\mathbf{r}_3}(E_2'-\omega_{21})G^*_{\mathbf{r}_1,\mathbf{r}_4}(E_2')\frac{\tilde{E}(\omega_1)\tilde{E}^*(\omega_2)}{E_2'-\omega_2+i0}e^{-i\omega_{12}t}+\text{c.c.} \tag{A8}$$

Here $\omega_{ij}=\omega_i-\omega_j$, $E_{ij}'=E_i'-E_j'$, and the single particle Green's function G is defined in Eq. (18). In deriving the last equality of the above equation, we have used the fact that $G_{\mathbf{r}_2,\mathbf{r}_3}(z)$ is an analytic function of z which has no poles in the upper half complex plane, therefore

$$\int dE_1'G_{\mathbf{r}_2,\mathbf{r}_3}(E_1')\frac{1}{E_2'-E_1'+\omega_1-\omega_2+i0}$$
$$=-2\pi i G_{\mathbf{r}_2,\mathbf{r}_3}(E_2'-\omega_{21}). \tag{A9}$$

Now we use the identity

$$\frac{1}{E_2'-\omega_2+i0}=\mathrm{PP}\frac{1}{E_2'-\omega_2}-i\pi\delta(E_2'-\omega_2), \tag{A10}$$

where PP denotes the principle part. Substituting Eq. (A10) into Eq. (A8), we see that the contribution of the principal part is imaginary and is canceled when the complex conjugate is added. Substituting the second term in the right-hand side of Eq. (A10) into Eq. (A8) and setting $\mathbf{r}_1\to\mathbf{r}_3$, $\mathbf{r}_2\to\mathbf{r}_1$, $\mathbf{r}_3\to\mathbf{r}_2$, we obtain Eq. (15).

APPENDIX B

In this appendix we derive Eq. (26) by using the ladder diagram approximation. We start with the Bethe–Salpeter equation with the ladder diagram approximation[17,25,26]

$$\phi(\mathbf{p},\mathbf{p}',\mathbf{q};\omega_1,\omega_2)\equiv MG(\mathbf{p}+\mathbf{q}/2,\omega_1)G^*(\mathbf{p}-\mathbf{q}/2,\omega_2)$$
$$\times\Delta(\mathbf{p}-\mathbf{p}')+\frac{1}{M}\sum_{\mathbf{p}''}G(\mathbf{p}+\mathbf{q}/2,\omega_1)$$
$$\times G^*(\mathbf{p}-\mathbf{q}/2,\omega_2)U(\omega_1,\omega_2)$$
$$\times\phi(\mathbf{p}'',\mathbf{p}',\mathbf{q};\omega_1,\omega_2). \tag{B1}$$

Here $G(\mathbf{p},\omega)$ and $\Delta(\mathbf{p})$ are defined in Eqs. (23) and (31). In Eq. (B1), $U(\omega_1,\omega_2)$ is given by the sum over all the single site diagrams (diagrams without crossing).[26] Iterating Eq. (B1), we have

$$\phi(\mathbf{p},\mathbf{p}',\mathbf{q};\omega_1,\omega_2)$$
$$=MG(\mathbf{p}+\mathbf{q}/2,\omega_1)G^*(\mathbf{p}-\mathbf{q}/2,\omega_2)\Delta(\mathbf{p}-\mathbf{p}')$$
$$+G(\mathbf{p}+\mathbf{q}/2,\omega_1)G^*(\mathbf{p}-\mathbf{q}/2,\omega_2)$$
$$\times G(\mathbf{p}'+\mathbf{q}/2,\omega_1)G^*(\mathbf{p}'-\mathbf{q}/2,\omega_2')$$
$$\times\frac{U(\omega_1,\omega_2)}{1-L(\mathbf{q},\omega_1,\omega_2)U(\omega_1,\omega_2)}, \tag{B2}$$

where $L(\mathbf{q};\omega_1,\omega_2)$ is defined is Eq. (27). To determine U, we used the following Ward identity:

$$\frac{1}{\omega_1-H^{\rm eff}+i0}-\left(\frac{1}{\omega_2-H^{\rm eff}+i0}\right)^+$$
$$=\frac{1}{\omega_1-H^{\rm eff}+i0}(\omega_{21}-2i\hat{\Gamma})\left(\frac{1}{\omega_2-H^{\rm eff}+i0}\right)^+. \tag{B3}$$

By taking trace and configurational averaging over both sides of the above equation, we have

$$\sum_{\mathbf{p}}[G(\mathbf{p},\omega_1)-G^*(\mathbf{p},\omega_2)]=\frac{1}{M}\sum_{\mathbf{p},\mathbf{p}'}\phi(\mathbf{p},\mathbf{p}',0;\omega_1,\omega_2)$$
$$\times[\omega_{21}-2i\Gamma(\mathbf{p}')], \tag{B4}$$

with summation over the first Brillouin zone. Here

$$|\mathbf{p}\rangle = \frac{1}{\sqrt{M}} e^{i\mathbf{p}\cdot\mathbf{r}} |\mathbf{r}\rangle, \tag{B5}$$

is a complete basis set. Substituting Eq. (B2) into Eq. (B4), we have

$$U(\omega_1,\omega_2) = \frac{1}{L(\mathbf{q}=0;\omega_1,\omega_2)} - \frac{\omega_{21} - i\Gamma_{12}(\omega_1,\omega_2)}{G(\omega_1) - G^*(\omega_2)}; \tag{B6}$$

where $\Gamma_{12}(\omega_1,\omega_2)$ and $G(\omega)$ are defined in Eqs. (28) and (29). Substituting Eq. (B6) into Eq. (B2) and setting $\mathbf{p}=\mathbf{k}_2$, $\mathbf{p}'=\mathbf{k}_1$, and $\mathbf{q}=0$, and then substituting into Eq. (21), we obtain Eq. (26).

[1] F. C. Spano, J. R. Kuklinski, and S. Mukamel, Phys. Rev. Lett. **65**, 211 (1990); J. Chem. Phys. **94**, 7534 (1991).
[2] F. C. Spano and S. Mukamel, J. Chem. Phys. **91**, 683 (1989).
[3] D. Mobius and H. Kuhn, Isr. J. Chem. **18**, 375 (1979); J. Appl. Phys. **64**, 5138 (1988).
[4] F. F. So, S. R. Forrest, Y. Q. Shi, and W. H. Steier, Appl. Phys. Lett. **56**, 674 (1990); F. F. So and S. R. Forrest, Phys. Rev. Lett. **66**, 2649 (1991).
[5] J. K. Jenkins and S. Mukamel, J. Chem. Phys. **98**, 7046 (1993).
[6] Y. Ohfuti and K. Cho, in *Proceedings of International Symposium on Science and Technology of Mesoscopic Structures*, Nara, Japan, 1991 (Springer, Berlin, 1991).
[7] S. Deboer and D. A. Wiersma, Chem. Phys. Lett. **165**, 45 (1990); S. Deboer, K. J. Vink, and D. A. Wiersma, *ibid.* **137**, 99 (1987).
[8] A. A. Muenter *et al.*, J. Phys. Chem. **96**, 2783 (1992); F. C. Spano *et al.*, A. A. Mol. Cryst. Liq. Cryst. **194**, 331 (1991).
[9] T. Tani, T. Suzumoto, K. Kemnitz, and K. Yoshihara, J. Phys. Chem. **96**, 2778 (1992).
[10] J. Grad, G. Hernandez, and S. Mukamel, Phys. Rev. A **37**, 3838 (1988).
[11] A. I. Zaitsev, V. A. Malyshev, and E. D. Trifinov, Sov. Phys. JETP **57**, 275 (1983).
[12] Y. C. Lee and P. S. Lee, Phys. Rev. B **10**, 344 (1974).
[13] V. Sundstrom, T. Gillbro, R. A. Gadonas, and A. Piskarskas, J. Chem. Phys. **89**, 2754 (1988).
[14] H. Haken and G. Strobl, Z. Phys. **262**, 135 (1973).
[15] D. Keller and C. Bustamante, J. Chem. Phys. **84**, 2961 (1986).
[16] H. Devoe, J. Chem. Phys. **41**, 393 (1964); **43**, 3199 (1965).
[17] N. Wang, J. A. Leegwater, and S. Mukamel, J. Chem. Phys. **98**, 5899 (1993).
[18] H. Fidder, J. Knoester, and D. A. Wiersma, J. Chem. Phys. **95**, 7880 (1991).
[19] L. Mower, Phys. Rev. **142**, 799 (1966).
[20] M. L. Goldberger and K. M. Watson, *Collision Theory* (Wiley, New York, 1969).
[21] J. Jortner and S. Mukamel, in *The World of Quantum Chemistry*, edited by R. Daudel and B. Pullman (Reidel, Dordrecht, 1974), pp. 145–209.
[22] A. S. Davydov, *Theory of Molecular Excitons* (Plenum, New York, 1971).
[23] S. Mukamel, Adv. Chem. Phys. **70**, 165 (1988).
[24] R. H. Lehmberg, Phys. Rev. A **2**, 883 (1970).
[25] D. Vollhardt and P. Wölfle, Phys. Rev. Lett. **45**, 842 (1980); Phys. Rev. B **22**, 4666 (1980).
[26] J. Kroha, Physica A **167**, 231 (1990).
[27] E. N. Economou, *Green's Functions in Quantum Physics* (Springer, New York, 1983).
[28] W. H. Press *et al.*, *Numerical Recipes* (Cambridge University, New York, 1988), p. 254.
[29] J. Knoester and S. Mukamel, Phys. Rep. **205**, 1 (1991).
[30] V. M. Agranovich and O. Dubovsky, Soviet Phys. JETP Lett. **3**, 223 (1966).
[31] U. Fano, Phys. Rev. **103**, 1202 (1956).
[32] J. J. Hopfield, Phys. Rev. **112**, 1555 (1958).
[33] M. Oritt and P. Kottis, Adv. Chem. Phys. **74**, 1 (1988).
[34] J. Knoester, Phys. Rev. Lett. **68**, 654 (1992).
[35] Y. J. Yan and S. Mukamel, J. Chem. Phys. **86**, 6085 (1987).